Numerical study of localized impurity in a Bose-Einstein condensate

Javed Akram[1,2,*] and Axel Pelster[3,†]

[1]*Institute für Theoretische Physik, Freie Universität Berlin, Arnimallee 14, 14195 Berlin, Germany*
[2]*Department of Physics, COMSATS, Institute of Information Technology, Islamabad, Pakistan*
[3]*Fachbereich Physik und Forschungszentrum OPTIMAS, Technische Universität Kaiserslautern, Kaiserslautern, Germany*
(Received 24 October 2015; published 4 March 2016)

Motivated by recent experiments, we investigate a single ^{133}Cs impurity in the center of a trapped ^{87}Rb Bose-Einstein condensate (BEC). Within a zero-temperature mean-field description we provide a one-dimensional physical intuitive model which involves two coupled differential equations for the condensate and the impurity wave function, which we solve numerically. With this we determine within the equilibrium phase diagram spanned by the intra- and interspecies coupling strength whether the impurity is localized at the trap center or expelled to the condensate border. In the former case we find that the impurity induces a bump or dip on the condensate for an attractive or a repulsive Rb-Cs interaction strength, respectively. Conversely, the condensate environment leads to an effective mass of the impurity which increases quadratically for small interspecies interaction strength. Afterwards, we investigate how the impurity imprint upon the condensate wave function evolves for two quench scenarios. At first we consider the case that the harmonic confinement is released. During the resulting time-of-flight expansion it turns out that the impurity-induced bump in the condensate wave function starts decaying marginally, whereas the dip decays with a characteristic time scale which decreases with increasing repulsive impurity-BEC interaction strength. Second, once the attractive or repulsive interspecies coupling constant is switched off, we find that white-shock waves or bisolitons emerge which both oscillate within the harmonic confinement with a characteristic frequency.

I. INTRODUCTION

Recent developments in theoretical and experimental research focus on controlling single-particle or few-particle impurities in an ultracold quantum gas in view of detecting and engineering strongly correlated quantum states [1–4]. This research direction paves the way for a huge number of proposals for novel applications. For example, a well-localized single-atom impurity with spin allows one to study the Kondo effect [5]. Dressed spin-down impurities in a spin-up Fermi sea of ultracold atoms even offer the possibility to investigate the quantum transport of spin impurity atoms through a strongly interacting Fermi gas [6,7]. Furthermore, realizations of a single trapped ion impurity in a Bose-Einstein condensate (BEC) features a spatial resolution on the micrometer scale which is advantageous in comparison with absorption imaging [8,9]. Atomtronics applications are envisioned with single atoms acting as switches for a macroscopic system in an atomtronics circuit [10]. Two impurity atoms immersed in a Bose-Einstein condensate can entangle through phonon exchange in a quantum gas [11] or individual qubits can be cooled preserving internal state coherence [12,13]. By adding impurities one by one, experimentalists can track, in principle, the transition from the one-body to the many-body regime, which ultimately yields information about cluster formation [14]. By implementing a single atom within a Bose-Einstein condensate also fundamental questions of quantum mechanics can be addressed with remarkable precision, for instance, to which extent a single impurity can act as a local and nondestructive probe for a strongly correlated quantum many-

body state [15,16]. In addition, the experimental achievement to trap a single impurity within a BEC [17–20] allows for investigating polaronic physics within the realm of ultracold quantum gases [21–24].

A convenient model to study the hybrid system of impurity within a BEC at zero temperature relies on the mean-field dynamics of two-coupled differential equations (DEs) for the condensate and the impurity wave function. For the sake of simplicity, we aim in this paper to analyze such a hybrid system in just one dimension. This is physically justified in the case that the confinement in two spatial dimensions is much larger than the third dimension, so the three-dimensional (3D) DEs reduce to a truly one-dimensional (1D) or a quasi-1D model. The first case requires transverse length scales on the order of or less than the atomic interaction length, which is realizable near a confinement-induced resonance [25–27] and allows for seminal experiments within the Tonks-Girardeau regime and the super-Tonks-Girardeau regime [28–30]. On the other hand, when the transverse confinement is larger than the atomic interaction strength, the DEs can be reduced to an effective quasi-1D model [31]. The trapping of a BEC in highly elongated optical and magnetic traps demonstrates that a quasi-1D BEC is experimentally realizable [29,32,33]. Note that such a mean-field description of a quasi-1D system at zero temperature neglects both quantum and thermal fluctuations which are known to be enhanced within a reduced dimensionality [33–37]. But if two-particle interaction strength and temperature are small enough, this quasi-1D mean-field model should provide a reasonable description.

Inspired by recent experiments [17–20], we propose and analyze a quasi-1D model of a hybrid system, which consists of a single ^{133}Cs impurity in a ^{87}Rb Bose-Einstein condensate. To this end, we start with defining the underlying quasi-1D model in Sec. II. As a result the effective 1D interspecies

———————
*javedakram@daad-alumni.de
†axel.pelster@physik.uni-kl.de

coupling strength depends not only on the 3D s-wave scattering length, but also on the transversal trap frequencies of cesium and rubidium, respectively. In the same section, we determine the equilibrium phase diagram spanned by the intra- and interspecies coupling strength and specify the regions where the impurity is localized at the trap center or expelled to the condensate border. Afterwards in Sec. III, we show for the former case that the impurity imprint upon the condensate wave function is either a bump or a dip, depending upon whether the effective impurity-BEC coupling strength is attractive or repulsive. Conversely, due to the presence of the condensate, the effective mass of the impurity turns out to depend quadratically upon a small interspecies coupling strength. Subsequently, Sec. IV discusses the dynamics of the impurity imprint upon the condensate wave function for two quench scenarios. After having released the trap, the resulting time-of-flight expansion shows that the impurity imprint marginally decreases for an attractive s-wave coupling but decreases for a repulsive s-wave scattering with a characteristic time scale which decreases with increasing the interspecies coupling strength. Furthermore, we investigate the emergence of white shock waves or gray or dark bisolitons when the initial negative or positive interspecies coupling constant is switched off. Section V summarizes our findings for the proposed quasi-1D model system in view of a possible experimental realization. Finally, in Appendix A we derive for the quasi-1D model the two underlying differential equations (1DDEs) for the condensate and the impurity wave function from a 3D setting.

II. QUASI-1D MODEL

We start with considering a BEC and an impurity confined in a harmonic trap. In the case of a strong transversal confinement one obtains an effective quasi-1D model which is described by two-coupled 1DDEs for the underlying condensate and impurity wave functions $\psi_B(z,t)$ and $\psi_I(z,t)$, respectively. The Appendix outlines how the 1D Lagrangian density (A5) is obtained from an original 3D setting by integrating out the two transversal degrees of freedom. The Euler-Lagrangian equations (A6) then reduce to the two coupled 1DDEs:

$$i\hbar\frac{\partial}{\partial t}\psi_B(z,t) = \left\{ -\frac{\hbar^2}{2m_B}\frac{\partial^2}{\partial z^2} + \frac{m_B\omega_z^2}{2}z^2 + G_{IB}\|\psi_I(z,t)\|^2 \right.$$
$$\left. + G_B\|\psi_B(z,t)\|^2 \right\}\psi_B(z,t), \quad (1)$$

$$i\hbar\frac{\partial}{\partial t}\psi_I(z,t) = \left\{ -\frac{\hbar^2}{2m_I}\frac{\partial^2}{\partial z^2} + \frac{m_I\omega_{Iz}^2}{2} + G_{BI}\|\psi_B(z,t)\|^2 \right\}$$
$$\times \psi_I(z,t). \quad (2)$$

On the right-hand side of Eqs. (1) and (2) the first term represents the kinetic energy of the BEC (impurity) atoms with mass m_B (m_I), the second term describes the potential energy term, the third term stands for the impurity-BEC coupling with the respective strengths $G_{IB} = g_{IB}$ and $G_{BI} = N_B g_{IB}$, and the last term in Eq. (1) represents the Rb-Rb two-particle interaction with strength $G_B = N_B g_B$. In the Appendix it is determined how g_B and g_{IB} depend on the s-wave scattering
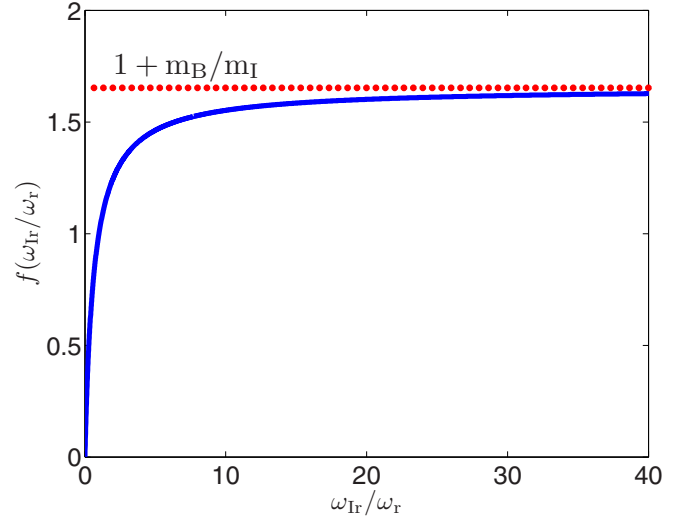

FIG. 1. Geometric function $f(\omega_{Ir}/\omega_r)$ reaches its maximum value at $1 + m_B/m_I$.

lengths a_B and a_{IB}. For intraspecies coupling one gets

$$g_B = 2a_B\hbar\omega_r, \quad (3)$$

whereas for interspecies coupling one obtains

$$g_{IB} = 2a_{IB}\hbar\omega_r f\left(\frac{\omega_{Ir}}{\omega_r}\right). \quad (4)$$

Here the geometric function

$$f\left(\frac{\omega_{Ir}}{\omega_r}\right) = \frac{1 + (m_B/m_I)}{1 + (m_B\omega_r)/(m_I\omega_{Ir})} \quad (5)$$

depends on the ratio of the trap frequencies as depicted in Fig. 1. Thus, $f(\omega_{Ir}/\omega_r)$ is monotonously increasing, equals to one for the present case $\omega_{Ir} = \omega_r$, and reaches its maximum value at $1 + m_B/m_I$ for the frequency ratio of about $\omega_{Ir}/\omega_r \geqslant 20$. In order to vary the impurity-BEC coupling strength there are, in principle, two possibilities according to Eq. (5): either the ratio of the radial trap frequencies is tuned as shown in Fig. 1, or the s-wave scattering length a_{IB} is modified with the use of a Feshbach resonance [17,38,39]. In order to make Eqs. (1) and (2) dimensionless we introduce the dimensionless time as $\tilde{t} = \omega_z t$, the dimensionless coordinate $\tilde{z} = z/l_z$, and the dimensionless wave function $\tilde{\psi} = \psi\sqrt{l_z}$, with the oscillator length $l_z = \sqrt{\hbar/(m_B\omega_z)}$. With this Eqs. (1) and (2) can be rewritten as follows:

$$i\frac{\partial}{\partial\tilde{t}}\tilde{\psi}_B(\tilde{z},\tilde{t}) = \left\{ -\frac{1}{2}\frac{\partial^2}{\partial\tilde{z}^2} + \frac{\tilde{z}^2}{2} + \tilde{G}_{IB}\|\tilde{\psi}_I(\tilde{z},\tilde{t})\|^2 \right.$$
$$\left. + \tilde{G}_B\|\tilde{\psi}_B(\tilde{z},\tilde{t})\|^2 \right\}\tilde{\psi}_B(\tilde{z},\tilde{t}), \quad (6)$$

$$i\frac{\partial}{\partial\tilde{t}}\tilde{\psi}_I(\tilde{z},\tilde{t}) = \left\{ -\frac{\tilde{\alpha}^2}{2}\frac{\partial^2}{\partial\tilde{z}^2} + \frac{\tilde{z}^2}{2\tilde{\alpha}^2} + \tilde{G}_{BI}\|\tilde{\psi}_B(\tilde{z},\tilde{t})\|^2 \right\}$$
$$\times \tilde{\psi}_I(\tilde{z},\tilde{t}), \quad (7)$$

where we have $\tilde{G}_B = N_B\tilde{g}_B$, $\tilde{G}_{IB} = \tilde{g}_{IB}$, and $\tilde{G}_{BI} = N_B\tilde{g}_{IB}$, with $\tilde{g}_B = g_B/(\hbar\omega_z l_z)$ and $\tilde{g}_{IB} = g_{IB}/(\hbar\omega_z l_z)$. Here $\tilde{\alpha} = l_{Iz}/l_z$ defines the ratio of the two oscillator lengths. Thus, we can
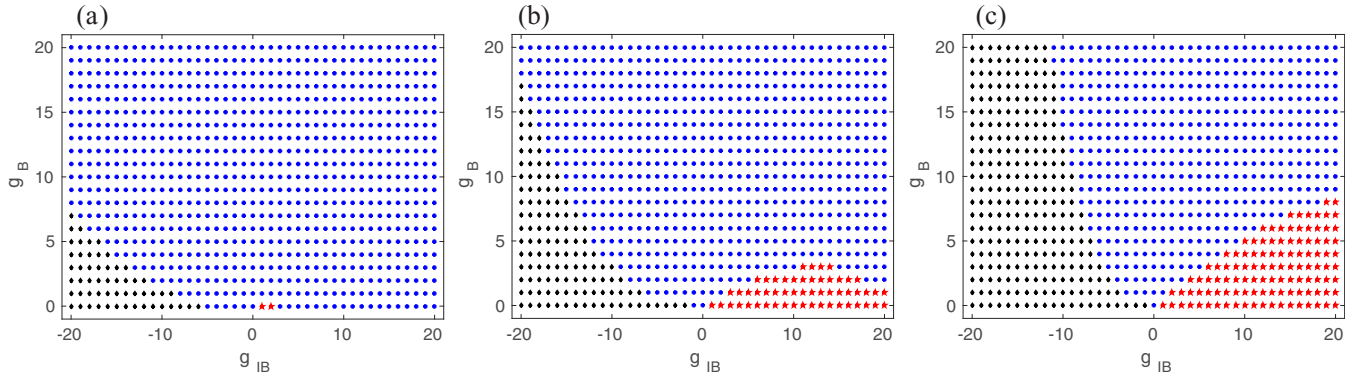
FIG. 2. Equilibrium phase diagram spanned by g_B and g_{IB} for (a) $N_B = 20$ (b) $N_B = 200$, and (c) $N_B = 800$. Impurity is localized at the trap center (blue) or expelled to the condensate border (red) together with the unstable region (black) in dimensionless units.

summarize that Eq. (6) is nothing but a standard Gross-Pitaevskii equation with an additional potential stemming from the impurity, whereas Eq. (7) is a typical Schrödinger wave equation with a potential originating from the BEC. From here on, we drop the tildes for simplicity.

Typically, a mixture of two species can occur in two different states, either it is miscible, i.e., both species overlap, or it is immiscible, i.e., the two species do not overlap [40,41]. In our case the equilibrium phase diagram is spanned by the coupling strengths g_B and g_{IB} and contains a region where the impurity is localized at the center and another region where the impurity is expelled to be localized at the border of the condensate. Note that a similar equilibrium phase diagram was studied for the homogeneous case with attractive interspecies s-wave scattering lengths in Ref. [42]. In order to investigate the physical regions of interest for our proposed model, we solve the two coupled 1DDEs (6) and (7) in imaginary time numerically by using the split-operator method [43–46], which yields the equilibrium phase diagram shown in Fig. 2. The blue region shows where the impurity is localized at the center of the BEC, the red region depicts that the impurity is displaced from the center to the border of the condensate, and finally, the black region represents the unstable region where the impurity and the condensate do not coexist.

In the rest of the paper, we are interested in the localization of the impurity at the center of the BEC; therefore, from now on, we only focus on the blue region in the equilibrium phase diagram of Fig. 2. In particular, we consider that the BEC consists of $N_B = 800$ ^{87}Rb atoms, for the dimensionless intraspecies couplings constant we assume $G_B = 16\,000$, and we let the ratio of the two oscillator lengths $\alpha = l_{Iz}/l_z$ have the value 0.808.

III. IMPURITY IMPRINT UPON STATIONARY CONDENSATE WAVE FUNCTION

In order to determine the impurity imprint on the condensate wave function in equilibrium we solve the two coupled 1DDEs numerically in imaginary time. In this way we find that the impurity leads to a bump or hole in the BEC density at the trap center for negative and positive values of g_{IB} as shown in Fig. 3. For increasing the attractive or repulsive interspecies coupling strength the bump or dip upon the condensate decreases or

increases. For the repulsive interspecies coupling strength, the impurity drills a dip in the BEC density which gets deeper and deeper until no more BEC atoms remain in the trap center and, finally, the BEC fully fragments into two parts as shown in Fig. 3(b) at the characteristic value $g_{IBc} = 110$. The width/height of the impurity wave function decreases or increases for increasing interspecies coupling constant $|g_{IB}|$, respectively, as shown in Figs. 3(c) and 3(d).

In view of a more detailed comparison, we describe the impurity imprint upon the condensate wave function $\psi_B(z)$ by the following two quantities. The first one is the impurity height/depth,

$$
\text{IHD} = \begin{cases} \|\psi_B(0)\|^2_{g_{IB}} - \|\psi_B(0)\|^2_{g_{IB}=0}, & g_{IB} \leqslant 0, \\ \text{Max}\big(\|\psi_B(z)\|^2_{g_{IB}}\big) - \|\psi_B(0)\|^2_{g_{IB}}, & g_{IB} \geqslant 0, \end{cases}
$$
(8)

and the second one is the impurity width IW, which we define as follows. For $g_{IB} \leqslant 0$ we use the full width half maximum,

$$
\|\psi(\text{IW}/2)\|^2_{g_{IB}} = \frac{\|\psi_B(0)\|^2_{g_{IB}} + \|\psi_B(0)\|^2_{g_{IB}=0}}{2}, \quad g_{IB} \leqslant 0,
$$
(9)

whereas for $g_{IB} \geqslant 0$ we define the equivalent width [47]:

$$
\text{IW} = \frac{2 I_0 z_{\text{Max}} - \int_{-z_{\text{Max}}}^{z_{\text{Max}}} \|\psi_B(z)\|^2_{g_{IB}} dz}{I_0 - \|\psi_B(0)\|^2_{g_{IB}}}, \quad g_{IB} \geqslant 0, \quad (10)
$$

where we have $I_0 = \text{Max}(\|\psi_B(z)\|^2_{g_{IB}})$. In Fig. 4(a) we plot the IHD for $g_{IB} > -10$, while $g_{IB} < -10$ is not a valid region for $g_B = 20$ according to Fig. 2(c). From Fig. 4(a) we read off that for $g_{IB} = 0$, i.e., when there is no impurity present, the impurity height/depth vanishes. The IHD quadratically increases for the repulsive interspecies coupling strength $0 < g_{IB} < 60$ and partially fragments the BEC until it reaches its marginally saturated value IHDc ≈ 0.025 for the characteristic interspecies coupling strength $g_{IBc} = 110$. In the case of $g_{IB} > g_{IBc}$, the impurity fully fragments the BEC into two parts as shown in Fig. 3(b). The impurity imprint width increases abruptly just before or after $g_{IB} = 0$ for attractive or repulsive interspecies coupling strength, respectively, as shown in Fig. 4(b). For an increasing repulsive impurity-BEC coupling strength the impurity width then decreases until it
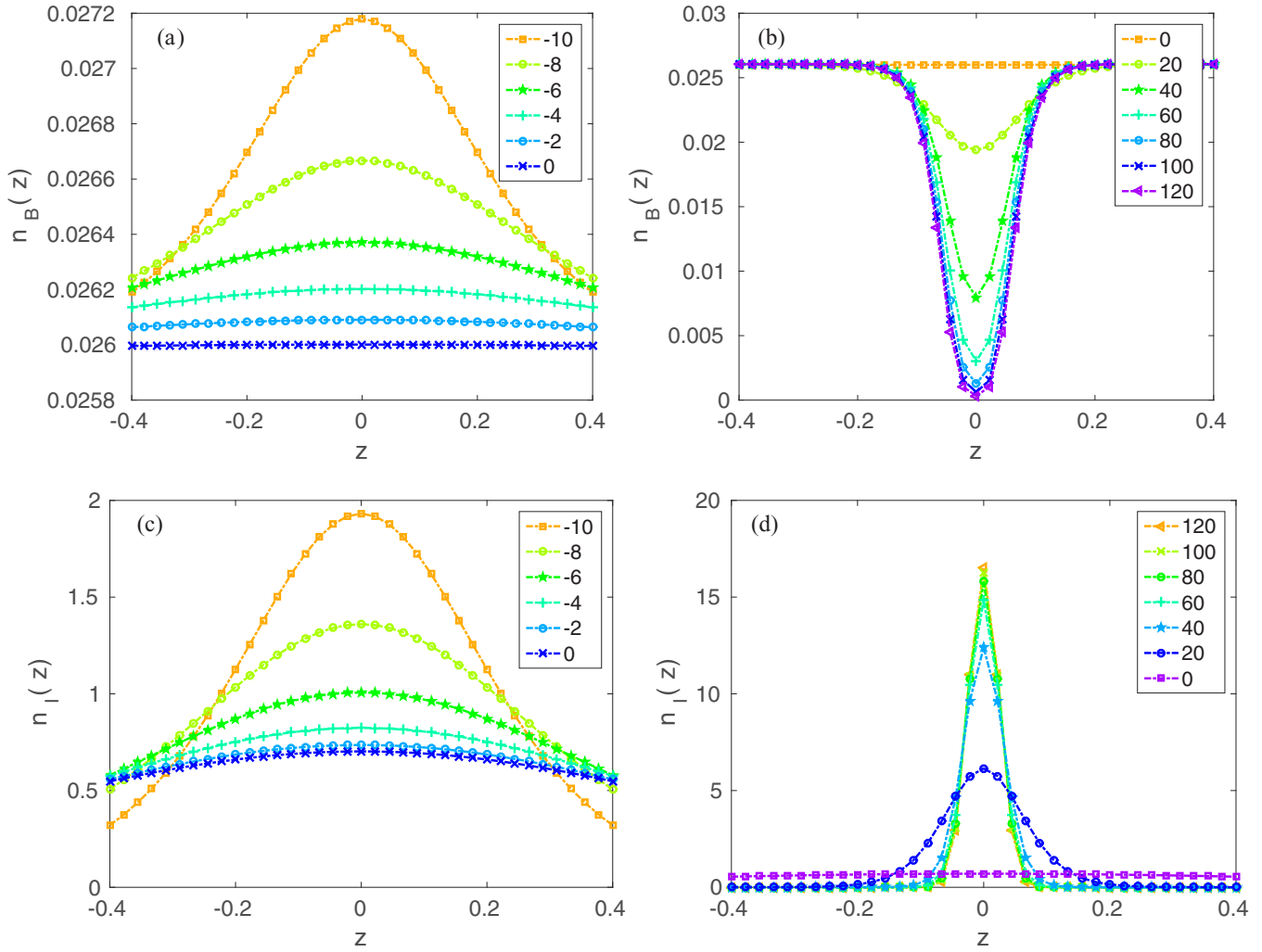
FIG. 3. Numerical density profile of BEC (a, b) and impurity (c, d) for the two-particle Rb-Rb coupling constant value $G_B = 16\,000$ and for interspecies coupling constants g_{IB} which increase from top to bottom according to the inlets. For increasing negative values of g_{IB} the impurity-induced bump (a) in the condensate wave function decreases, whereas for positive values the corresponding dip (b) increases in dimensionless units.
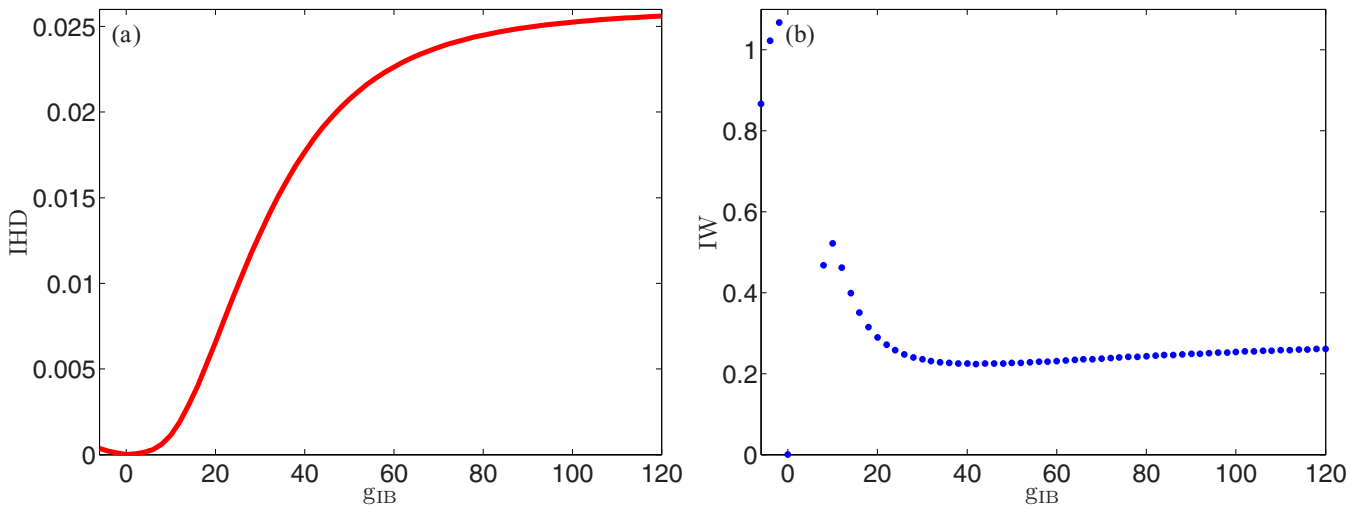

FIG. 4. (a) Height/depth and (b) width of the impurity bump/dip according to Eqs. (8)–(10) versus the impurity-BEC coupling constant g_{IB} for the BEC coupling constant $G_B = 16\,000$ calculated numerically by solving 1DDEs (6) and (7) in dimensionless units.
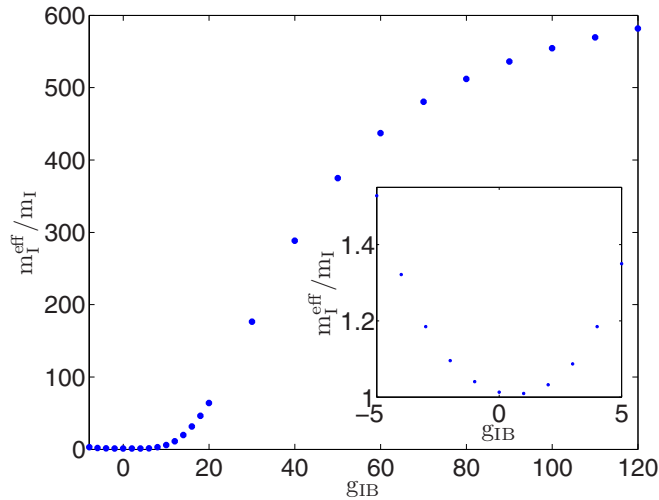
FIG. 5. Effective mass of ^{133}Cs impurity versus the impurity-BEC coupling strength g_{IB}. The inset shows that the effective mass increases quadratically for small impurity-BEC coupling strength g_{IB} in dimensionless units.

reaches the interspecies coupling strength $g_{IB} = 30$; later on it marginally increases until the characteristic interspecies coupling strength $g_{IBc} = 110$, where we have IWc ≈ 0.23.

The effective mass of the impurity is defined as $m_I^{eff} = \hbar/(l_{Iz}^2 \omega_z)$, where the impurity oscillator length $l_{Iz} = \sqrt{2}\sigma$ follows from the standard deviation $\sigma = \sqrt{\langle z^2 \rangle - \langle z \rangle^2}$, with $\langle \bullet \rangle = \int \bullet |\psi_I(z)|^2 dz$ denoting the expectation value. Figure 5 shows the ratio of the effective mass of the ^{133}Cs impurity with respect to the bare mass m_I, which increases quadratically for interspecies coupling strength $-5 < g_{IB} < 5$ as shown in the inset of Fig. 5, and becomes marginally saturated for interspecies coupling strength $g_{IB} > g_{IBc}$. Note that our results for the effective mass of the impurity are restricted to the mean-field regime. In order to go beyond and include the impact of quantum fluctuations, one would need to investigate polaron physics [21,22,24,48].

IV. IMPURITY IMPRINT UPON CONDENSATE DYNAMICS

In an experiment, any imprint of the impurity upon the condensate wave function could only be detected dynamically. Thus, it is of high interest to study theoretically whether the impurity imprint, which we have found and analyzed for the stationary case in the previous section, remains present also during the dynamical evolution of the condensate wave function. To this end, we explore two quench scenarios numerically in more detail. The first one is the standard time-of-flight (TOF) expansion after having switched off the external trap when the interspecies interaction is still present. In the second case we consider the inverted situation that the impurity-BEC interaction is suddenly switched off within a remaining harmonic confinement, which turns out to give rise to the emergence of wave packets or bisolitons depending on whether the initial interspecies interaction strength is attractive or repulsive.

A. Time-of-flight expansion

TOF absorption pictures represent an important diagnostic tool to analyze dilute quantum gases since the field's inception. By suddenly turning off the magnetic trap, the atom cloud expands nonballistically with a dynamics which is determined by both the momentum distribution of the atoms at the instance, when the confining potential is switched off, and by interatomic interactions [49,50]. We have investigated the time-of-flight expansion dynamics of the BEC with impurity by solving numerically the two coupled 1DDEs, Eqs. (6) and (7), and analyzing the resulting evolution of both the condensate and the impurity wave function. It turns out that, despite the continuous broadening of the condensate density, its impurity imprint remains qualitatively preserved both for attractive and repulsive interspecies interaction strengths, respectively. Therefore, we focus a more quantitative discussion upon the dynamics of the corresponding impurity height/depth and width.

For an attractive Rb-Cs coupling strength, it turns out that the impurity imprint even remains approximately constant in the time-of-flight, as is shown explicitly in Fig. 6(a) for the
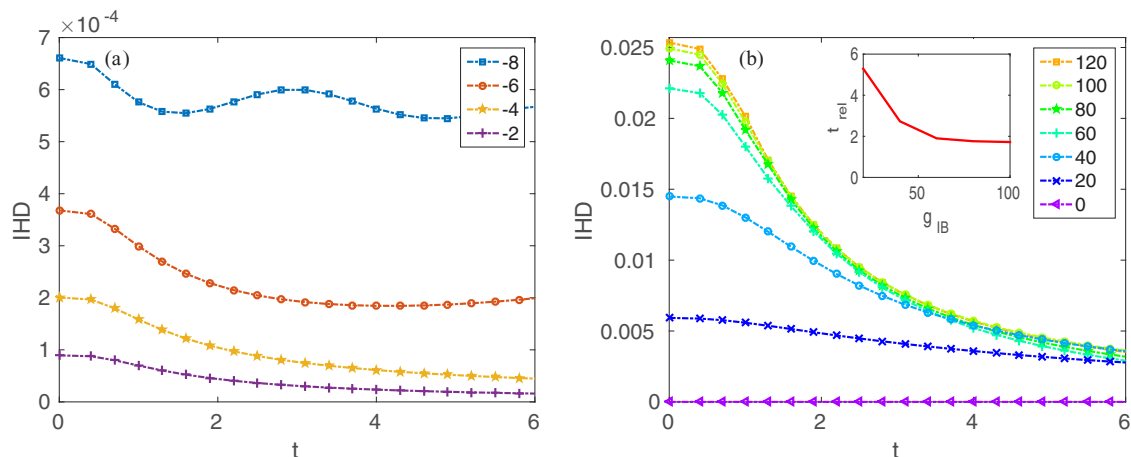

FIG. 6. Impurity imprint height/depth after having released the trap versus time for (a) increasing negative and (b) decreasing positive values of the impurity-BEC coupling constant g_{IB} from top to bottom. Inset: Relaxation time t_{rel} decreases with increasing g_{IB} in dimensionless units.
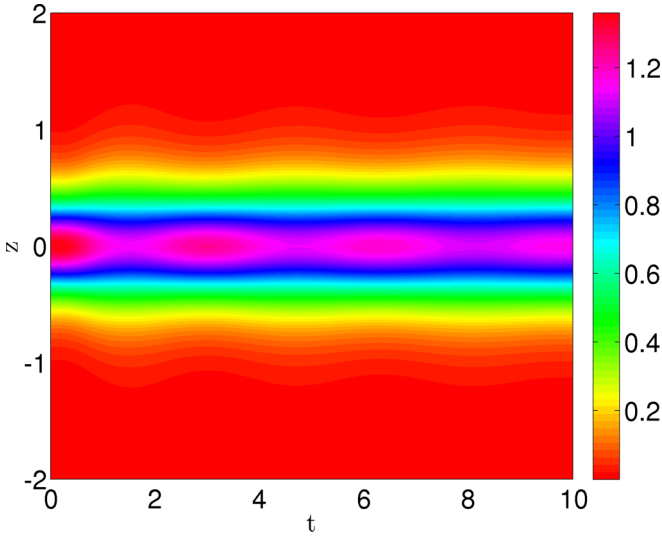
FIG. 7. Dynamics of the impurity density represented in color scale after having switched off the harmonic trap for the initial $g_{\mathrm{IB}} = -8$ for the BEC coupling strength $G_{\mathrm{B}} = 16\,000$ in dimensionless units.

IHD, which marginally decreases for $t \gg 0$. As shown in Fig. 6(a) for smaller attractive interspecies coupling strength, we observe the crumbling breathing of the impurity upon the IHD as discussed recently for the Bose-Hubbard model [51]. For the attractive interspecies coupling strength $g_{\mathrm{IB}} = -8$ the dynamics of the impurity density is shown in Fig. 7, which clearly reflects the crumbling breathing of the impurity at the center of the BEC. In the case of the IW, we find that the IW starts increasing marginally for smaller values of attractive interspecies coupling strength and increases linearly for larger attractive interspecies coupling strength g_{IB} as shown in Fig. 8.

In the case of a repulsive interspecies interaction, the IHD decays with a characteristic time scale as shown in Fig. 6(b).
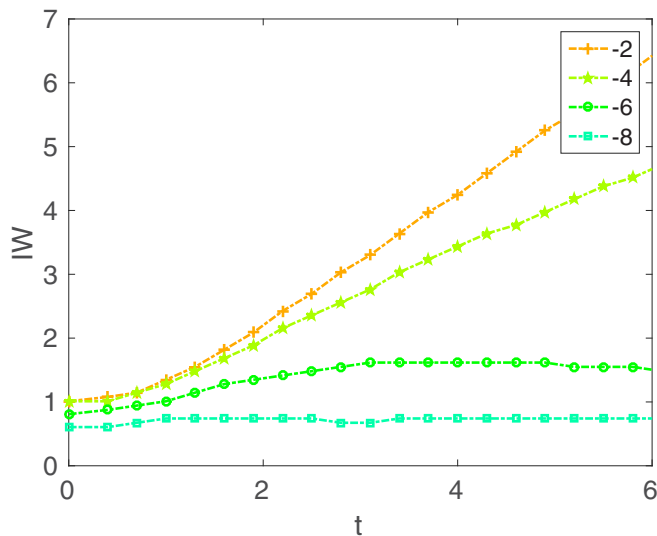

FIG. 8. Impurity imprint width after having released the trap versus time for decreasing positive values of the impurity-BEC coupling constant g_{IB} from top to bottom in dimensionless units.
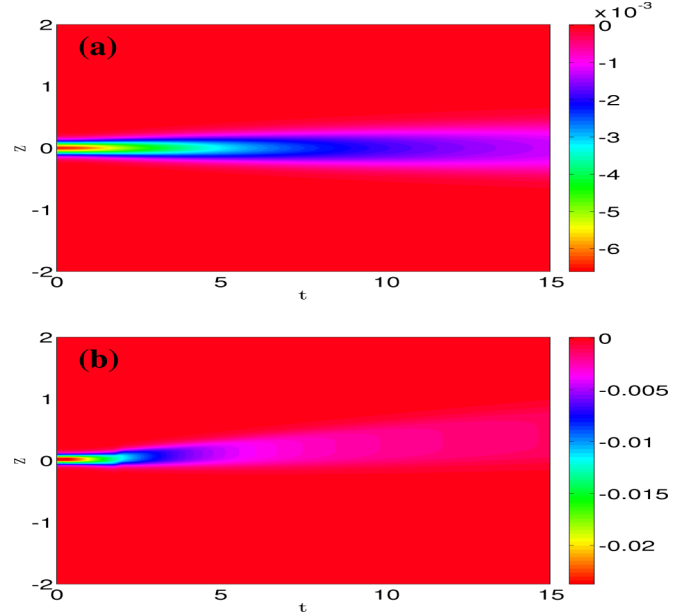

FIG. 9. Coherent matter-wave time-of-flight evolution of the depleted density $\|\psi_{\mathrm{B}}(z,t)\|_{\mathrm{DD}}^2 = \|\psi_{\mathrm{B}}(z,t)\|_{g_{\mathrm{IB}}}^2 - \|\psi_{\mathrm{B}}(z,t)\|_{g_{\mathrm{IB}}=0}^2$ represented in color scale after having switched off the trap for the BEC coupling constant $G_{\mathrm{B}} = 16\,000$: (a) $g_{\mathrm{IB}} = 20$ and (b) $g_{\mathrm{IB}} = 80$ in dimensionless units.

Defining that relaxation time t_{rel} according to $\mathrm{IHD}(t_{\mathrm{rel}}) = \mathrm{IHD}(0)/2$, the inlet reveals that the impurity imprint depth relaxes with a shorter time scale for increasing repulsive impurity-BEC coupling strength. This physical picture is confirmed by the time-of-flight evolution of the depleted density depicted in Fig. 9. At the beginning of TOF the impurity-imprint remains at first constant, then the imprint width expands and the imprint height decays faster for a larger interspecies coupling strength. In Fig. 9 we plotted the time-of-flight of the depleted density of the BEC for two cases. For the repulsive interspecies coupling strength $g_{\mathrm{IB}} = 20$ we observe that the impurity imprint decays marginally from its equilibrium value as shown in Fig. 6(b) and the impurity remains localized at the trap center as shown in Fig. 9(a). On the other hand, for the larger value of the repulsive interspecies coupling strength $g_{\mathrm{IB}} = 80$, the impurity imprint decays from its equilibrium value as shown in Fig. 6(b) and at the same time the impurity is expelled from the center of the BEC as shown in Fig. 9(b). With this we conclude that for a small enough repulsive interspecies coupling strength the impurity survives in the center of the BEC for larger times.

B. Wave packets versus solitons

Due to their quantum coherence, BECs exhibit rich and complex dynamic patterns, which range from the celebrated matter-wave interference of two colliding condensates [52] over Faraday waves [53,54] to the particlelike excitations of solitons [55–63]. For our proposed quasi-1D model of a BEC with an impurity we investigated the dynamics of the condensate wave function which emerges after having switched off the interspecies coupling strength. Both for an initial attractive and repulsive interspecies coupling strength
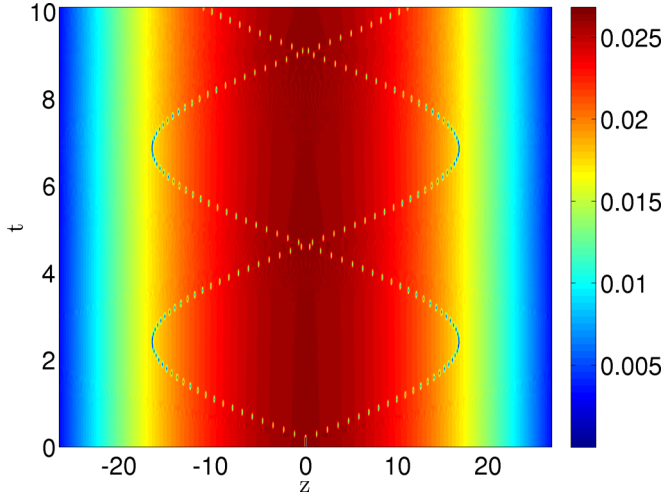
FIG. 10. Density profile of the BEC represented in color scale after having switched off the impurity-BEC coupling constant for initial $g_{IB} = 120$ for the BEC coupling constant $G_B = 16\,000$ in dimensionless units.

g_{IB} we observe that two excitations of the condensate are created at the impurity position, which travel in opposite directions with the same center-of-mass speed, are reflected at the trap boundaries and then collide at the impurity position as shown exemplarily in Fig. 10 for the initial $g_{IB} = 120$ and $G_B = 16\,000$. These excitations qualitatively retain their shape despite the collision at the impurity position. All these findings are not yet conclusive to decide whether these excitations represent wave packets in the absence of dispersion or solitons. Therefore, we investigate their dynamics in more detail, by determining their center-of-mass motion via [62]

$$\bar{z}_{L,R}(t) = \frac{\int_{-\infty,0}^{0,\infty} z \left(\|\psi_B(z,t)\|^2_{g_{IB}} - \|\psi_B(z,t)\|^2_{g_{IB}=0} \right) dz}{\int_{-\infty,0}^{0,\infty} \left(\|\psi_B(z,t)\|^2_{g_{IB}} - \|\psi_B(z,t)\|^2_{g_{IB}=0} \right) dz}, \quad (11)$$

which are plotted in Fig. 11. Note that the mean positions $\bar{z}_L$ and $\bar{z}_R$ of the excitations are uncertain in the region where they collide. Nevertheless Fig. 11 demonstrates that the excitations oscillate with the frequency $\omega = 2\pi \times 35.7$ Hz irrespective of the sign and size of g_{IB}. As we have assumed the trap frequency $\omega_z = 2\pi \times 50$ Hz, we obtain the ratio $\omega/\omega_z \approx 0.714$, which is quite close to $\omega/\omega_z = 1/\sqrt{2} \approx 0.707$. Despite these similarities of the cases of an initial attractive and repulsive interspecies coupling constant g_{IB}, we observe one significant difference. Whereas the oscillation amplitudes of the excitations do not depend on the value of the initial $g_{IB} < 0$ according to Fig. 11(a), we find decreasing oscillation amplitudes of the excitations with increasing the initial $g_{IB} > 0$ in Fig. 11(b). Such an amplitude dependence on the initial condition is characteristic for gray or dark solitons according to Ref. [58]. This particlelike interpretation of the excitations agrees with the other theoretical prediction of Ref. [58] that gray or dark solitons oscillate in a harmonic confinement with the frequency $\omega/\omega_z = 1/\sqrt{2}$, which was already confirmed in the Hamburg experiment of Ref. [60] and is also seen in Fig. 11. Conversely, for an initial attractive interspecies coupling constant the excitations cannot be identified with bright solitons as the dynamics is governed by a Gross-Pitaevskii equation with a repulsive two-particle interaction. Here the excitations have to be interpreted as wave packets which move without any dispersion; thus, for $g_{IB} < 0$ the excitations propagate like sound waves in the BEC [62–64]. Thus, we conclude that switching off the interspecies coupling constant leads for $g_{IB} < 0$ and $g_{IB} > 0$ to physically different situations. For an initial attractive RbCs coupling constant we generate wave packets which correspond to white-shock waves [65], whereas for the corresponding repulsive case bisolitons emerge [66,67], which are due to the collision of the two partially or fully fragmented parts of the condensate. When the shock wave approaches the trap boundary, it penetrates into the trap potential, which leads to a change of its shape, and later it recovers its shape. Therefore we see a small kink in the center-of-mass position amplitude at time $t \sim 2.5$ as
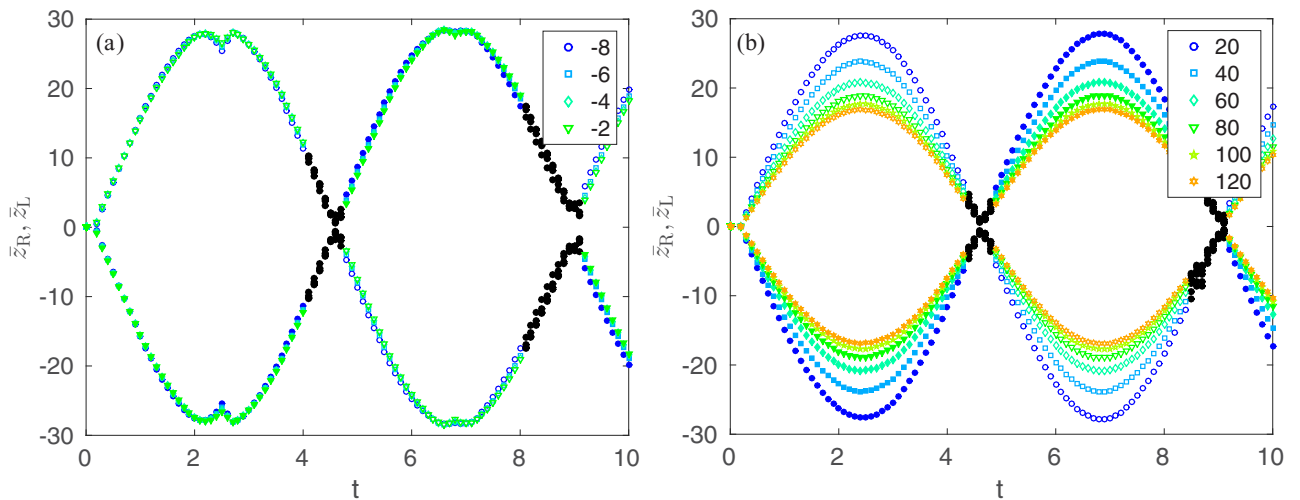

FIG. 11. Center-of-mass positions of excitations $\bar{z}_L$ (solid circles) and $\bar{z}_R$ (empty circles) according to Eq. (11) versus time after having switched off (a) negative decreasing and (b) positive increasing values of g_{IB} from top to bottom. Black solid circles represent the region of colliding excitations, where mean positions are not perfectly detectable in dimensionless units.

shown in Fig. 11(a). On the other hand the solitary wave is characterized by preserving its shape so it is reflected back from the potential boundary without changing its shape. Thus we do not see any kink in Fig. 11(b). Note that it can be shown in our proposed system that gray bisolitons are generated for a partially fragmented BEC, i.e., the impurity-BEC coupling strength $g_{IB} < g_{IBc}$. On the other hand the dark bisolitons turn out to be only generated for $g_{IB} > g_{IBc}$, where the BEC is fully fragmented into two parts at equilibrium. Recently, we have observed that bisolitons trains are generated in the traditional harmonic trap with an additional dimple trap [62]. We emphasize that besides many practical applications of the impurity-BEC system, someone can also generate solitons by considering an impurity as a drilling appliance to fragment the BEC, which allows one to study solitons' physics in the condensate.

V. SUMMARY AND CONCLUSION

In the present work we studied within a quasi-1D model numerically how a single impurity in the center of a trapped BEC affects the condensate wave function. At first, we investigated the equilibrium properties of that hybrid system by numerically solving the underlying two coupled 1DDEs (6) and (7) with the imaginary-time propagation method. For an increasing attractive or repulsive Rb-Cs interaction strength it turns out that the impurity imprint bump or dip decreases or increases quadratically and reaches its marginally saturated value after $g_{IBc} = 110$. Later we found that the impurity imprint width increases abruptly for increasing the attractive or repulsive Rb-Cs interaction strength, but for the repulsive case it reaches a marginally saturated value for $g_{IB} > g_{IBc}$. Beyond the characteristic value g_{IBc}, the BEC fragments into two parts and, if g_{IB} is increased beyond g_{IBc}, the impurity yields a condensate wave function whose impurity width increases further, although the impurity height/depth remains constant. Afterwards, we investigated the impurity imprint upon the condensate dynamics for two quench scenarios.

At first, we considered the release of the harmonic confinement, which leads to a time-of-flight expansion and found that the impurity imprint upon the condensate decays slowly for small valves of the attractive and repulsive interspecies coupling strength. This result suggests that it might be experimentally easier to observe the impurity imprint for small attractive or repulsive coupling constant g_{IB}. We also observed the decaying breathing of the impurity at the center of the condensate for small attractive Rb-Cs coupling strength. Additionally, we found for stronger repulsive interspecies coupling strength that the ^{87}Rb atoms repel the single ^{133}Cs impurity from the center. In an experiment one has to take into account that inelastic collisions lead to two- and three-body losses of the condensate atoms [68,69]. As such inelastic collisions are enhanced for a higher BEC density, they play a vital role for an attractive interspecies coupling, when the condensate density has a bump at the impurity position, but are negligible in the repulsive case with the dip in the wave function.

In addition, we analyzed the condensate dynamics after having switched off the interspecies coupling strength. This case turned out to be an interesting laboratory in which to study the physical similarities and differences of bright shock waves and gray and dark bisolitons, which emerge for an initial negative and positive interspecies coupling constant g_{IB}, respectively. We consider the astonishing observation that the oscillation frequencies of both the shock waves and the soliton coincide to be an artifact of the harmonic confinement. Additionally, we also found that the generation of gray and dark bisolitons is a generic phenomenon on collisions of partially and fully fragmented BECs, respectively, which is strongly depending upon the equilibrium values of the impurity wave function height and width.

APPENDIX

We start with the fact that the underlying equations for describing an impurity immersed in a BEC can be formulated in terms of the Hamilton principle of least action with the action functional $\mathcal{A}_{3D} = \int dt \int \mathcal{L}_{3D} d^3 r$, where the Lagrangian density reads as follows for three dimensions:

$$\mathcal{L}_{3D} = \sum_{j=B,I} N_j \left\{ \frac{i\hbar}{2} \left[\psi_j^\star(\mathbf{r},t) \frac{\partial \psi_j(\mathbf{r},t)}{\partial t} - \psi_j(\mathbf{r},t) \frac{\partial \psi_j^\star(\mathbf{r},t)}{\partial t} \right] \right.$$
$$+ \frac{\hbar^2}{2m_j} \psi_j^\star(\mathbf{r},t) \triangle \psi_j(\mathbf{r},t) - V_j(\mathbf{r}) \psi_j^\star(\mathbf{r},t) \psi_j(\mathbf{r},t)$$
$$\left. - \frac{N_j g_j^{3D}}{2} \|\psi_j(\mathbf{r},t)\|^4 \right\}$$
$$- N_B N_I g_{IB}^{3D} \|\psi_I(\mathbf{r},t)\|^2 \|\psi_B(\mathbf{r},t)\|^2. \tag{A1}$$

Here $\psi_B(\mathbf{r},t)$ and $\psi_I(\mathbf{r},t)$ describe the BEC and the impurity wave function with $\mathbf{r} = (x, y, z)$, and $V_B(\mathbf{r}) = m_B \omega_z^2 z^2/2 + m_B \omega_r^2 (x^2 + y^2)/2$ and $V_I(\mathbf{r}) = m_I \omega_{Iz}^2 z^2/2 + m_I \omega_{Ir}^2 (x^2 + y^2)/2$ denote the 3D harmonic potential for the bosons and the ^{133}Cs impurity. The 3D ^{87}Rb coupling constant reads $g_B^{3D} = 4\pi \hbar^2 a_B/m_B$, where the s-wave scattering length is $a_B = 94.7 a_0$ with the Bohr radius a_0 and m_B stands for the mass of the ^{87}Rb atom, while the 3D ^{133}Cs coupling constant reads $g_I^{3D} = 0$, because there is only one single ^{133}Cs impurity atom present in the system, i.e., $N_I = 1$. The 3D effective Rb-Cs coupling constant is $g_{IB}^{3D} = 2\pi \hbar^2 a_{IB}/m_{IB}$, where $m_{IB} = m_I m_B/(m_I + m_B)$ is the reduced mass of two species, m_I is the mass of the ^{133}Cs atom, and $a_{IB} = 650 a_0$ represents the effective Rb-Cs s-wave scattering length [17]. We assume an effective 1D setting with $\omega_z \ll \omega_r$, so we decompose the BEC wave function $\psi_B(\mathbf{r},t) = \psi_B(z,t) \phi_B(\mathbf{r}_\perp,t)$, with $\mathbf{r}_\perp = (x, y)$

and

$$\phi_{\text{B}}(\mathbf{r}_\perp, t) = \frac{e^{-\frac{x^2+y^2}{2l_{\text{r}}^2}}}{\sqrt{\pi}l_{\text{r}}} e^{-i\omega_{\text{r}}t}. \tag{A2}$$

Furthermore, we assume that the single impurity in the center of the BEC is trapped by a harmonic potential with $\omega_{\text{Iz}} \ll \omega_{\text{Ir}}$. Thus, we perform a similar decomposition of the impurity wave function $\psi_{\text{I}}(\mathbf{r},t) = \psi_{\text{I}}(z,t)\phi_{\text{I}}(\mathbf{r}_\perp,t)$, with

$$\phi_{\text{I}}(\mathbf{r}_\perp, t) = \frac{e^{-\frac{x^2+y^2}{2l_{\text{rI}}^2}}}{\sqrt{\pi}l_{\text{rI}}} e^{-i\omega_{\text{rI}}t}. \tag{A3}$$

Here $l_{\text{r}} = \sqrt{\hbar/(m_{\text{B}}\omega_{\text{r}})}$ and $l_{\text{Ir}} = \sqrt{\hbar/(m_{\text{I}}\omega_{\text{Ir}})}$ denote the oscillator lengths in the radial direction for the BEC and the impurity. For the experimentally realistic trap frequencies $\omega_{\text{r}} = \omega_{\text{Ir}} = 2\pi \times 0.179$ kHz $\ll \omega_{\text{z}} = \omega_{\text{Iz}} = 2\pi \times 0.050$ kHz [18], these radial oscillator lengths amount to the values $l_{\text{r}} = 15\,190.8a_0$ and $l_{\text{Ir}} = 12\,279.0a_0$ for the BEC and the impurity, respectively. In order to distinguish between the weakly interacting quasi-1D regime and the strongly interacting Tonks-Girardeau regime, Petrov *et al.* [26] introduced a dimensionless quantity which involves both the longitudinal and the transversal trap size as well as the scattering length:

$$\alpha = 2a_{\text{B}} \frac{l_{\text{z}}}{l_{\text{r}}^2}. \tag{A4}$$

By using the abovementioned experimental parameters, we get the dimensionless quantity $\alpha = 0.023$, so we are far in the weakly interacting regime, where the Gross-Pitaevskii mean-field theory is applicable (see also Fig. 5 of Ref. [36] and Refs. [70,71]). Therefore, we can follow Ref. [31] and integrate out the two transversal dimensions of our 3D Lagrangian according to $\mathcal{L}_{\text{1D}} = \int_{-\infty}^{\infty}\int_{-\infty}^{\infty}\mathcal{L}_{\text{3D}}dxdy$. After some algebra, the resulting quasi-1D Lagrangian reads

$$\mathcal{L}_{\text{1D}} = \sum_{j=\text{B,I}} N_j \left\{ \frac{i\hbar}{2}\left[\psi_j^\star(z,t)\frac{\partial\psi_j(z,t)}{\partial t} - \psi_j(z,t)\frac{\partial\psi_j^\star(z,t)}{\partial t}\right] \right.$$
$$+ \frac{\hbar^2}{2m_j}\psi_j^\star(z,t)\triangle\psi_j(z,t) - V_j(z)\psi_j^\star(z,t)\psi_j(z,t)$$
$$\left. - \frac{N_j g_j}{2}\|\psi_j(z,t)\|^4 \right\}$$
$$- N_{\text{B}}N_{\text{I}}g_{\text{IB}}\|\psi_{\text{I}}(z,t)\|^2\|\psi_{\text{B}}(z,t)\|^2, \tag{A5}$$

where $V_{\text{B,I}}(z) = m_{\text{B,I}}\omega_{\text{z,Iz}}^2 z^2/2$ represents the 1D harmonic potential for the BEC and for the impurity, the one-dimensional intraspecies coupling strength g_{B} is given by Eq. (3), and the interspecies coupling strength g_{IB} turns out to be Eq. (4). The two coupled time-dependent differential equations follow from the action $\mathcal{A}_{\text{1D}} = \int_{-\infty}^{\infty}\int_{-\infty}^{\infty}\mathcal{L}_{\text{1D}}dzdt$ and by using the Euler-Lagrangian equation

$$\frac{\partial\mathcal{L}_{\text{1D}}}{\partial\psi_j^\star(z,t)} - \frac{\partial}{\partial z}\frac{\partial\mathcal{L}_{\text{1D}}}{\partial\frac{\partial\psi_j^\star(z,t)}{\partial z}} - \frac{\partial}{\partial t}\frac{\partial\mathcal{L}_{\text{1D}}}{\partial\frac{\partial\psi_j^\star(z,t)}{\partial t}} = 0. \tag{A6}$$

Inserting the 1D Lagrangian density (A5), after some algebra we obtain the two coupled 1DDEs (1) and (2).

---

[1] T. Gericke, P. Wurtz, D. Reitz, T. Langen, and H. Ott, Nat. Phys. **4**, 949 (2008).

[2] W. S. Bakr, J. I. Gillen, A. Peng, S. Folling, and M. Greiner, Nature (London) **462**, 74 (2009).

[3] J. F. Sherson, C. Weitenberg, M. Endres, M. Cheneau, I. Bloch, and S. Kuhr, Nature (London) **467**, 68 (2010).

[4] F. Serwane, G. Zürn, T. Lompe, T. B. Ottenstein, A. N. Wenz, and S. Jochim, Science **332**, 336 (2011).

[5] A. V. Gorshkov, M. Hermele, V. Gurarie, C. Xu, P. S. Julienne, J. Ye, P. Zoller, E. Demler, M. D. Lukin, and A. M. Rey, Nat. Phys. **6**, 289 (2010).

[6] A. Schirotzek, C.-H. Wu, A. Sommer, and M. W. Zwierlein, Phys. Rev. Lett. **102**, 230402 (2009).

[7] S. Palzer, C. Zipkes, C. Sias, and M. Köhl, Phys. Rev. Lett. **103**, 150601 (2009).

[8] C. Zipkes, S. Palzer, C. Sias, and M. Köhl, Nature (London) **464**, 388 (2010).

[9] S. Schmid, A. Härter, and J. H. Denschlag, Phys. Rev. Lett. **105**, 133202 (2010).

[10] A. Micheli, A. J. Daley, D. Jaksch, and P. Zoller, Phys. Rev. Lett. **93**, 140408 (2004).

[11] A. Klein and M. Fleischhauer, Phys. Rev. A **71**, 033605 (2005).

[12] A. J. Daley, P. O. Fedichev, and P. Zoller, Phys. Rev. A **69**, 022306 (2004).

[13] A. Griessner, A. J. Daley, S. R. Clark, D. Jaksch, and P. Zoller, Phys. Rev. Lett. **97**, 220403 (2006).

[14] A. Klein, M. Bruderer, S. R. Clark, and D. Jaksch, New J. Phys. **9**, 411 (2007).

[15] H. T. Ng and S. Bose, Phys. Rev. A **78**, 023610 (2008).

[16] J. B. Balewski, A. T. Krupp, A. Gaj, D. Peter, H. P. Buchler, R. Low, S. Hofferberth, and T. Pfau, Nature (London) **502**, 664 (2013).

[17] A. D. Lercher, T. Takekoshi, M. Debatin, B. Schuster, R. Rameshan, F. Ferlaino, R. Grimm, and H.-C. Nägerl, Eur. Phys. J. D **65**, 3 (2011).

[18] N. Spethmann, F. Kindermann, S. John, C. Weber, D. Meschede, and A. Widera, Appl. Phys. B **106**, 513 (2012).

[19] N. Spethmann, F. Kindermann, S. John, C. Weber, D. Meschede, and A. Widera, Phys. Rev. Lett. **109**, 235301 (2012).

[20] M. Hohmann, F. Kindermann, B. Gänger, T. Lausch, D. Mayer, F. Schmidt, and A. Widera, EPJ Quantum Technol. **2**, 23 (2015).

[21] W. Casteels, J. Tempere, and J. T. Devreese, Phys. Rev. A **84**, 063612 (2011).

[22] D. H. Santamore and E. Timmermans, New J. Phys. **13**, 103029 (2011).

[23] J. Catani, G. Lamporesi, D. Naik, M. Gring, M. Inguscio, F. Minardi, A. Kantian, and T. Giamarchi, Phys. Rev. A **85**, 023623 (2012).

[24] F. Grusdt and E. Demler, arXiv:1510.04934 (2015).

[25] M. Olshanii, Phys. Rev. Lett. **81**, 938 (1998).

[26] D. S. Petrov, G. V. Shlyapnikov, and J. T. M. Walraven, Phys. Rev. Lett. **85**, 3745 (2000).

[27] T. Bergeman, M. G. Moore, and M. Olshanii, Phys. Rev. Lett. **91**, 163201 (2003).

[28] B. Paredes, A. Widera, V. Murg, O. Mandel, S. Fölling, I. Cirac, G. V. Shlyapnikov, T. W. Hänsch, and I. Bloch, Nature (London) **429**, 277 (2004).

[29] T. Kinoshita, T. Wenger, and D. S. Weiss, Science **305**, 1125 (2004).

[30] E. Haller, M. Gustavsson, M. J. Mark, J. G. Danzl, R. Hart, G. Pupillo, and H.-C. Nägerl, Science **325**, 1224 (2009).

[31] A. Kamchatnov, J. Exp. Theor. Phys. **98**, 908 (2004).

[32] K. Bongs, S. Burger, S. Dettmer, D. Hellweg, J. Arlt, W. Ertmer, and K. Sengstock, Phys. Rev. A **63**, 031602 (2001).

[33] A. Görlitz, J. M. Vogels, A. E. Leanhardt, C. Raman, T. L. Gustavson, J. R. Abo-Shaeer, A. P. Chikkatur, S. Gupta, S. Inouye, T. Rosenband, and W. Ketterle, Phys. Rev. Lett. **87**, 130402 (2001).

[34] F. Schreck, L. Khaykovich, K. L. Corwin, G. Ferrari, T. Bourdel, J. Cubizolles, and C. Salomon, Phys. Rev. Lett. **87**, 080403 (2001).

[35] S. Dettmer, D. Hellweg, P. Ryytty, J. J. Arlt, W. Ertmer, K. Sengstock, D. S. Petrov, G. V. Shlyapnikov, H. Kreutzmann, L. Santos, and M. Lewenstein, Phys. Rev. Lett. **87**, 160406 (2001).

[36] D. Petrov, D. M. Gangardt, and G. V. Shlyapnikov, J. Phys. IV **116**, 5 (2004).

[37] J. Esteve, J.-B. Trebbia, T. Schumm, A. Aspect, C. I. Westbrook, and I. Bouchoule, Phys. Rev. Lett. **96**, 130403 (2006).

[38] K. Pilch, A. D. Lange, A. Prantner, G. Kerner, F. Ferlaino, H.-C. Nägerl, and R. Grimm, Phys. Rev. A **79**, 042718 (2009).

[39] T. Takekoshi, M. Debatin, R. Rameshan, F. Ferlaino, R. Grimm, H.-C. Nägerl, C. R. Le Sueur, J. M. Hutson, P. S. Julienne, S. Kotochigova, and E. Tiemann, Phys. Rev. A **85**, 032506 (2012).

[40] H. Pu and N. P. Bigelow, Phys. Rev. Lett. **80**, 1130 (1998).

[41] A. Sartori and A. Recati, Eur. Phys. J. D **67**, 260 (2013).

[42] R. M. Kalas and D. Blume, Phys. Rev. A **73**, 043608 (2006).

[43] D. Vudragović, I. Vidanović, A. Balaž, P. Muruganandam, and S. K. Adhikari, Comput. Phys. Commun. **183**, 2021 (2012).

[44] R. K. Kumar, L. E. Young-S., D. Vudragović, A. Balaž, P. Muruganandam, and S. Adhikari, Comput. Phys. Commun. **195**, 117 (2015).

[45] V. Lončar, A. Balaž, A. Bogojević, S. Škrbić, P. Muruganandam, and S. K. Adhikari, Comput. Phys. Commun. **200**, 406 (2016).

[46] B. Satarić, V. Slavnić, A. Belić, A. Balaž, P. Muruganandam, and S. K. Adhikari, Comput. Phys. Commun. **200**, 411 (2016).

[47] B. Carroll and D. Ostlie, *An Introduction to Modern Astrophysics* (Addison-Wesley, Boston, 2007).

[48] J. Tempere, W. Casteels, M. K. Oberthaler, S. Knoop, E. Timmermans, and J. T. Devreese, Phys. Rev. B **80**, 184504 (2009).

[49] M.-O. Mewes, M. R. Andrews, N. J. van Druten, D. M. Kurn, D. S. Durfee, and W. Ketterle, Phys. Rev. Lett. **77**, 416 (1996).

[50] S. Inouye, T. Pfau, S. Gupta, A. P. Chikkatur, A. Görlitz, D. E. Pritchard, and W. Ketterle, Nature (London) **402**, 641 (1999).

[51] S. Peotta, D. Rossini, M. Polini, F. Minardi, and R. Fazio, Phys. Rev. Lett. **110**, 015302 (2013).

[52] M. R. Andrews, C. G. Townsend, H.-J. Miesner, D. S. Durfee, D. M. Kurn, and W. Ketterle, Science **275**, 637 (1997).

[53] P. Engels, C. Atherton, and M. A. Hoefer, Phys. Rev. Lett. **98**, 095301 (2007).

[54] A. Balaž and A. I. Nicolin, Phys. Rev. A **85**, 023613 (2012).

[55] W. P. Reinhardt and C. W. Clark, J. Phys. B **30**, L785 (1997).

[56] Y. S. Kivshar and B. Luther-Davies, Phys. Rep. **298**, 81 (1998).

[57] T. F. Scott, R. J. Ballagh, and K. Burnett, J. Phys. B **31**, L329 (1998).

[58] T. Busch and J. R. Anglin, Phys. Rev. Lett. **84**, 2298 (2000).

[59] J. Ruostekoski, B. Kneer, W. P. Schleich, and G. Rempe, Phys. Rev. A **63**, 043613 (2001).

[60] C. Becker, S. Stellmer, P. Soltan-Panahi, S. Dorscher, M. Baumert, E. M. Richter, J. Kronjager, K. Bongs, and K. Sengstock, Nat. Phys. **4**, 496 (2008).

[61] I. Shomroni, E. Lahoud, S. Levy, and J. Steinhauer, Nat. Phys. **5**, 193 (2009).

[62] J. Akram and A. Pelster, arXiv:1508.05482 (2015).

[63] J. Akram and A. Pelster, Phys. Rev. A **93**, 023606 (2016).

[64] M. R. Andrews, D. M. Kurn, H.-J. Miesner, D. S. Durfee, C. G. Townsend, S. Inouye, and W. Ketterle, Phys. Rev. Lett. **79**, 553 (1997).

[65] B. Damski, Phys. Rev. A **73**, 043601 (2006).

[66] K. E. Strecker, G. B. Partridge, A. G. Truscott, and R. G. Hulet, Nature (London) **417**, 150 (2002).

[67] U. Al Khawaja, H. T. C. Stoof, R. G. Hulet, K. E. Strecker, and G. B. Partridge, Phys. Rev. Lett. **89**, 200404 (2002).

[68] S. L. Cornish, N. R. Claussen, J. L. Roberts, E. A. Cornell, and C. E. Wieman, Phys. Rev. Lett. **85**, 1795 (2000).

[69] R. Carretero-González, D. J. Frantzeskakis, and P. G. Kevrekidis, Nonlinearity **21**, R139 (2008).

[70] W. Ketterle and N. J. van Druten, Phys. Rev. A **54**, 656 (1996).

[71] L. Carr, M. Leung, and W. Reinhardt, J. Phys. B **33**, 3983 (2000).